Non-isothermal, non Newtonian flow of polymers in complex geometries

10

Non-isothermal, non Newtonian flow of polymers in complex geometries

C. W. M. Sitters and W. A. M. Brekelmans – Faculty of Mechanical Engineering, Eindhoven University of Technology, The Netherlands.

Introduction

Injection moulding is an important industrial process for the series production of complex thin walled or small thermoplastic products. Driven by the development of new polymers with a superior quality, the tendency is present to manufacture very accurate and/or heavily loaded products by injection moulding, which formerly were made with other techniques. The quality requirements raise so high that the manufacturing experience becomes inadequate. Therefore it is desirable to develop numerical tools, which at least will approximate the influence of material properties and process conditions on the final quality. This paper is confined to the analysis of the filling stage of the process, where a polymer is injected into a complex three-dimensional cavity, with a small but varying gap height. The viscosity of the polymer depends on temperature, shear rate and pressure. Solidification of the polymer at the cooled walls of the mould is taken into account. The solidification temperature is pressure dependent and asymmetrical cooling is allowed. The specific volume and the thermodynamic properties are temperature and pressure dependent. For these properties curve fits and/or tabulated experimental data can be used.
In the continuum approach the solid-liquid interface is regarded as a discontinuity surface, where in principle, all quantities can change discontinuously. Therefore, besides the conservation laws, also the jump relations for mass, momentum and energy are important. Also see Becker and Bürger (1975) and Müller (1985). The numerical process is based on a mixed finite element/finite

difference method, which has been introduced by Hieber and Shen (1980). After the thin film (Hele Shaw) approximation (Richardson, 1972; Schlichting, 1982) the pressure is assumed to be independent of the coordinate in the direction of the channel height. Consequently, it is sufficient to evaluate the pressure at the midplane of the mould. This is done by a finite element procedure in order to prevent problems due to the complexity of the geometry of the midplane. The velocities and the temperatures essentially remain three-dimensional and are solved with a finite difference scheme. The finite difference grid lines are applied in the direction of the channel height at the vertices of the elements. The mesh is spatially fixed and contains the whole midplane of the cavity. During the simulation of the process, the flow front moves through this mesh.
The problem is solved in a number of time increments. After each time step, the new position of the flow front is calculated. At the flow front the mesh is adapted in such a manner that a proper mesh results. All relevant equations are solved iteratively. After convergence, a new time increment is made.

Governing equations resulting from the thin film approximation
A heat conducting viscous fluid is considered. The aim is to predict the pressure p, the velocity $\vec{v}$ and the temperature T during the process. In the fluid the Cauchy stress tensor σ is given by: $\sigma = -pI + 2\eta D^d$, where η is the viscosity and D^d is equal to the deviatoric part of the deformation rate tensor D, with $D = (\vec{\nabla}\vec{v} + (\vec{\nabla}\vec{v})^c)/2$. The heat conduction is governed by Fourier's law, expressing that for the heat flux vector $\vec{q}$ holds: $\vec{q} = -\lambda \vec{\nabla}T$, with λ the heat conduction coefficient.
The cavity is a three-dimensional weakly curved channel. At the midplane a unit normal $\vec{e}_z$ is defined. In the direction of $\vec{e}_z$ a coordinate z is chosen, which is zero at the midplane.

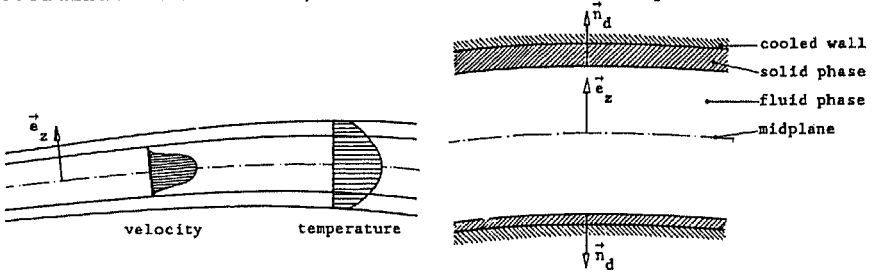

Fig. 1 Geometry, velocity and temperature field

In the fluid and solid phases the conservation laws for mass, momentum and energy are valid. The solid-liquid interfaces are regarded as discontinuity surfaces, with normal $\vec{n}_d$ pointing from the fluid into the solid phase. On these surfaces the jump

relations with respect to mass, momentum and energy are applied. The channel height is assumed to be a weakly varying function of the midplane coordinates. This will be valid for the solidified layers too. Therefore within a good approximation $\vec{n}_d = \pm \vec{e}_z$. An arbitrary vector $\vec{a}$ can be decomposed into a normal vector $\vec{a}\cdot\vec{e}_z\vec{e}_z = a_z\vec{e}_z$ and a tangent vector $\vec{a}^{**} = \vec{a} - a_z\vec{e}_z$ perpendicular to $\vec{e}_z$. Similarly the (midplane) gradient operator is introduced: $\vec{\nabla}^{**} = \vec{\nabla} - \vec{e}_z \frac{\partial}{\partial z}$. It can be derived: $\mathrm{tr}(D) = \vec{\nabla}^{**}\cdot\vec{v}^{**} + \partial v_z/\partial z$. In the fluid the velocity and temperature gradients in z-direction are large compared to the midplane gradients. The component of the velocity in z-direction is also relatively small. Neglecting small contributions it can be deduced: $D^d = \frac{1}{2}\frac{\partial}{\partial z}(\vec{v}^{**}\vec{e}_z + \vec{e}_z\vec{v}^{**})$, with $(\mathrm{tr}(D))^2 \ll D^d:D^d$. In the solid phase only a velocity component in z-direction ($\vec{v} = v_z\vec{e}_z$) is assumed. The velocity $\vec{v}^{**}$ at the solid-liquid interfaces is zero. For the temperature gradients in both solid and fluid phases it follows: $\vec{\nabla}T = \vec{e}_z \frac{\partial T}{\partial z}$.

Balance equations in the fluid phase

The continuity equation reads:

$$\vec{\nabla}^{**}\cdot\vec{v}^{**} + \frac{\partial v_z}{\partial z} = -\frac{\dot{\rho}}{\rho} = -\frac{1}{\rho}\left(\frac{\partial \rho}{\partial t} + \frac{\partial \rho}{\partial z} v_z + \vec{\nabla}^{**}\rho\cdot\vec{v}^{**}\right) \qquad (1)$$

where ρ is the mass density.
Due to the very high viscosity, the inertial and gravity forces can be neglected (Re $\ll$ 1 and Re $\ll$ Fr). The momentum equation reduces to $\vec{\nabla}\cdot\boldsymbol{\sigma} = \vec{0}$. Using the constitutive equation for $\boldsymbol{\sigma}$ and the approximations discussed above, this leads to:

$$\vec{\nabla}^{**}p = \frac{\partial}{\partial z}\left(\eta\frac{\partial \vec{v}^{**}}{\partial z}\right) \quad ; \quad \frac{\partial p}{\partial z} = 0 \qquad (2)$$

Assuming the specific internal energy ϵ and ρ to be functions of p and T only, for the material derivative of ϵ it follows: $\dot{\epsilon} = c_p\dot{T} + p\dot{\rho}/\rho^2 + T(\partial\rho/\partial T)_p\,\dot{p}/\rho^2$. Taking this into account the energy equation, neglecting the source term, reads:

$$\rho c_p\left(\frac{\partial T}{\partial t} + \frac{\partial T}{\partial z}v_z + \vec{\nabla}^{**}T\cdot\vec{v}^{**}\right) = \frac{\partial}{\partial z}\left(\lambda\frac{\partial T}{\partial z}\right) + \eta\dot{\gamma}^2 - \frac{T}{\rho}\left(\frac{\partial \rho}{\partial T}\right)_p\left(\frac{\partial p}{\partial t} + \vec{\nabla}^{**}p\cdot\vec{v}^{**}\right) \qquad (3)$$

where the shear rate $\dot{\gamma}$ is defined as: $\dot{\gamma} = \sqrt{(2D^d:D^d)} = |\frac{\partial \vec{v}^*}{\partial z}|$

Balance equations in the solid phase

The continuity equation reads:

$$\frac{\partial v_z}{\partial z} = -\frac{\dot{\rho}}{\rho} = -\frac{1}{\rho}(\frac{\partial \rho}{\partial t} + \frac{\partial \rho}{\partial z} v_z) \tag{4}$$

With the assumption that the pressure in z-direction is constant too, the relevant momentum equation becomes:

$$\frac{\partial p}{\partial z} = 0 \tag{5}$$

In the solid phase no viscous dissipation occurs and $\vec{v}^* = \vec{0}$, which reduces the energy equation to:

$$\rho c_p (\frac{\partial T}{\partial t} + \frac{\partial T}{\partial z} v_z) = \frac{\partial}{\partial z}(\lambda \frac{\partial T}{\partial z}) - \frac{T}{\rho}(\frac{\partial \rho}{\partial T})_p \frac{\partial p}{\partial t} \tag{6}$$

Jump relations at the solid-liquid interface

The jump relation for the continuity equation reads:

$$\rho^s(u_z - v_z^s) - \rho^f(u_z - v_z^f) = 0 \tag{7}$$

The superscripts s en f indicate the solid and fluid phase, respectively, u_z is the not material bounded velocity component of the solid-liquid interface. For the jump relation with respect to the momentum equation, within a good approximation, holds:

$$p^s - p^f = 0 \tag{8}$$

The jump relation for energy (Stefan equation) can be written as:

$$(\Gamma + \frac{\rho^s - \rho^f}{\rho^s \rho^f} p)\rho^s(u_z - v_z^s) - \lambda^s(\frac{\partial T}{\partial z})^s + \lambda^f(\frac{\partial T}{\partial z})^f = 0 \tag{9}$$

where $\Gamma = (\epsilon^s - \epsilon^f)$ equals the phase transition heat. For the detailed derivation of the equations above see Sitters (1988).

Derivation of the pressure problem

Since the pressure p does not depend on the z-coordinate, the first relation of (2) can be integrated twice with respect to z. The domain of the fluid phase in z-direction is bounded by the

two solidified layers $\alpha^- \leq z \leq \alpha^+$. For $z = \alpha^+$ and $z = \alpha^-$ holds $\vec{v}^* = \vec{0}$. Using these boundary conditions it can be deduced:

$$\frac{\partial \vec{v}^*}{\partial z} = \frac{1}{\eta}(z - \frac{J_1}{J_0})\vec{\nabla}^* p \tag{10}$$

$$\vec{v}^* = (\int_{\alpha^-}^{z} \frac{1}{\eta}(z - \frac{J_1}{J_0})dz)\vec{\nabla}^* p \tag{11}$$

with:

$$J_0 = \int_{\alpha^-}^{\alpha^+} \frac{1}{\eta}dz \quad ; \quad J_1 = \int_{\alpha^-}^{\alpha^+} \frac{z}{\eta}dz \tag{12}$$

Integrating $\vec{v}^*$ over the channel height results in the following useful relation:

$$\int_{\alpha^-}^{\alpha^+} \vec{v}^* dz = - S\vec{\nabla}^* p \tag{13}$$

where:

$$S = J_2 - \frac{J_1}{J_0} J_1 \quad ; \quad J_2 = \int_{\alpha^-}^{\alpha^+} \frac{z^2}{\eta}dz \tag{14}$$

The continuity equation (1) will be integrated with respect to z too. Combining this with (13) for the pressure is found:

$$\vec{\nabla}^* \cdot (S\vec{\nabla}^* p) = v_z(\alpha^+) - v_z(\alpha^-) + \int_{\alpha^-}^{\alpha^+} \frac{\dot{\rho}}{\rho}dz \tag{15}$$

This equation will be solved by the finite element technique.

Numerical procedure

The finite element mesh is spatially fixed and contains the whole midplane of the cavity. The finite difference grid in z-direction

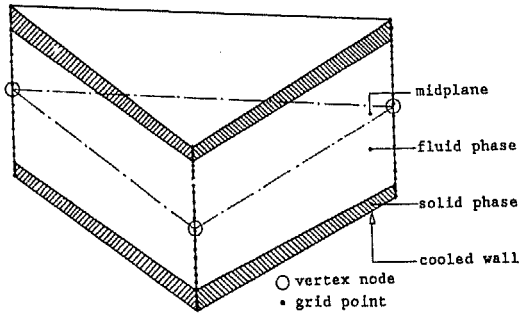

Fig. 2 Grid lines at the vertices of a finite element

is applied at every vertex node covering the fluid and the two solidified layers against the cooled walls.
As the problem is transient the solution is obtained in a number of time steps. After each time step, the new position of the flow front is calculated. On the sides of the elements which are intersected by the flow front, temporary nodes will be created and the covered part of the intersected elements will be divided into one or more sub-elements, in such a manner that a proper mesh is obtained for the whole actual domain. An element may contain different flow fronts (Fig. 3 and 4).

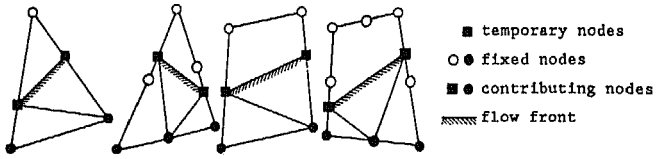

Fig. 3 Sub-divisions into three node elements

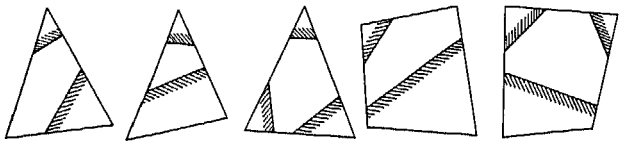

Fig. 4 Elements with several flow fronts

The complete flow front consists of a number of connected edges of sub-elements. The velocity of the flow front is taken equal to the average velocity $\vec{v}_a^{**}$ in the connected sub-element. This velocity is perpendicular to the flow front. During a time increment Δt the displacement $\Delta\vec{x}^{**}$ of each line segment can be determined, using an explicit Euler integration scheme: $\Delta\vec{x}^{**} = \vec{v}_a^{**}(t-\Delta t)\Delta t$. A detailed description of the determination of the flow front, on a curved midplane, is given by Sitters (1988).
When the new flow front is obtained an iteration process will be started, to solve all relevant equations successively. As a first estimation of the important quantities, the values calculated at the previous time will be chosen. For the values of the quantities in the grid points, which just have entered the fluid, appropriate estimations are made. The iteration process globally is composed of the steps mentioned below.

1) Solution of the pressure equation (15), resulting in a new estimation for p, $|\vec{\nabla}^{**}p|$, $\dot{\gamma}$ and $|\vec{v}^{**}|$ in every node. Subsequently the viscosity η and the mass density ρ are updated.
2) Solution of the continuity equations (1), (4) and (7), supplying a new estimation of the velocity component v_z.
3) Updating of the thermal conductivity λ and specific heat

capacity c_p. Solution of the energy equations in the solid and liquid domains to derive a new temperature distribution.

4) Calculation of the new positions α^+ and α^- of the solid-liquid interfaces on all grid lines, from the jump relation with respect to energy (9).
5) Convergence check with respect to pressure, temperature and positions of the solidified layers.

The several steps of the iteration process will be briefly discussed below.

Pressure problem

Equation (15) is non-linear with respect to p and will be solved using a Picard iteration scheme, where S and the right handside are evaluated from the results of the previous iteration cycle. At the flow front the pressure equals zero. The boundary conditions at the walls of the mould are satisfied easily. The injection areas are modeled by point sources, situated at vertex nodes of the finite elements. Doing so the prescribed volume fluxes can be taken into account.
After the pressure is obtained in the nodes, the mean pressure gradient $\vec{\nabla}^* p$ is calculated in every element. In all vertex nodes in the fluid $|\vec{\nabla}^* p|$ will be computed, using an averaging procedure over all the connected elements. Also $\dot{\gamma}$ and $|\vec{v}^*|$ in every vertex node will be calculated from (10) and (11) as a function of z.

Continuity equations

The continuity equations will be solved by finite difference schemes. The spatial time derivatives $\partial\rho/\partial t$ in (1) and (4) will be approximated by a backwards difference scheme.
For the continuity equation in the solid layer, at the wall of the mould with position $z = -h/2$, the derivatives with respect to z will be approximated implicitly from the values of the related quantities at two adjacent grid points. For the grid point located at the wall holds $v_z = 0$. The discretized equation (4) can be solved for the other grid points, successively, resulting in a new estimation for the velocity component v_z, including the velocity at the solid-liquid interface v_z^s. For the other solidified layer the procedure is analogue.
From the jump relation (7) the values $v_z^f(\alpha^-)$ and $v_z^f(\alpha^+)$, which are the boundary conditions for the continuity equation in the liquid, can be determined. For ρ^s, ρ^f and v_z^s the updated values are chosen. The non-material velocity u_z of the solid-liquid interface is calculated in the previous iteration cycle. In order to specify the jump in certain quantities at the solid-liquid

interface, two coinciding grid points are defined, one in the fluid and one in the solid phase.
In the fluid phase, the derivatives with respect to z will be approximated with an implicit central difference scheme. The terms $\vec{\nabla}^{*}\rho\cdot\vec{v}^{*}$ and $\vec{\nabla}^{*}\cdot\vec{v}^{*}\vec{v}^{*}$ will be evaluated, based on a backwards difference scheme, using an up-stream flow path.

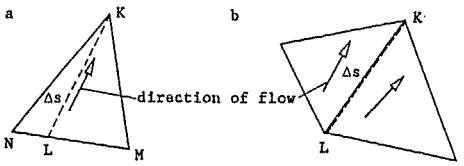

Fig. 5 The up-stream flow paths

In the grid points of the line situated in K (Fig. 5), v_z will be determined. The up-stream flow path is indicated by the dashed line. In Fig. 5a a grid line L is defined at the intersection of the flow path and the opposite element edge. The distance between K and L is equal to Δs. The values of the desired quantities in the points of L are obtained by linear interpolation between the values of the corresponding grid points of M and N. In Fig. 5b is indicated that in several cases a flow path along an element edge is a reasonable assumption.
The discretized equation (1) is of the first order, however, with two boundary conditions at the solid-liquid interfaces. In order to satisfy both of these conditions a least-square method is applied. This method produces a linear tridiagonal system of equations which can be solved with a standard technique, providing a new approximation of v_z in the fluid domain.

Energy equations

Only the solution of the energy equation in the fluid phase will be discussed, because in this equation all the relevant terms are present. The boundary conditions in the fluid phase are the estimated solidification temperatures at the solid-liquid interfaces. In the solid phase apart from a solidification temperature the wall temperature is prescribed.
The spatial time derivatives $\partial T/\partial t$ and $\partial p/\partial t$ will be handled in the same manner as $\partial\rho/\partial t$ above. The derivative $\partial T/\partial z$ and the conduction term $\partial(\lambda\partial T/\partial z)/\partial z$ will be discretized implicitly by a central difference scheme. The most crucial point appears to be the evaluation of the convective term $\vec{\nabla}^{*}T.\vec{v}^{*}$. Numerical experiments have shown that, in order to obtain any stable solution, this term has to be approximated with a backwards difference scheme (Hieber and Shen (1980) also mentioned this). The numerical scheme using the up-stream flow paths, as discussed above, can be applied succesfully. The evaluation of $\vec{\nabla}^{*}p\cdot\vec{v}^{*}$ will be done similarly.

For every grid line in the fluid as well as in the solid phases three tridiagonal matrix equations can be derived. With the boundary conditions these equations can be solved, producing a new temperature distribution.

Positions of the solid-liquid interfaces

The positions of the solid-liquid interfaces will be calculated directly from the jump relation with respect to energy (9). The velocity u_z of the interface can be approximated by a backwards difference scheme. For the solid-liquid interface belonging to $z = \alpha^-$ it follows: $u_z = (\alpha^-(t) - \alpha^-(t-\Delta t))/\Delta t$. Substitution of this relation in (9) results in an equation from which the present position $\alpha^-(t)$ of the interface can be obtained. Because of the high non-linearity of this equation, it will be solved by a bisection method (Sitters, (1988)). The position of the solid-liquid interface for $z = \alpha^+$ is calculated analogously.

Results and conclusions

Numerical experiments have shown that the velocity component v_z cannot be evaluated accurately enough. The inaccuracy of v_z probably can be explained from the poor approximation of $\vec{\nabla}^*\cdot\vec{v}^*$ in (1) which, according to (11) is proportional to $\vec{\nabla}^*\cdot\vec{\nabla}^* p$. the discretization chosen for p is unsuitable to obtain a reliable estimation for this term. Applying a higher order element (parabolic instead of linear) will not reduce the problem, because $\vec{\nabla}^* p$ remains discontinuous across the element sides. This raises the suggestion that an element has to be formulated, with at least $\vec{\nabla}^* p$ continuity across the element sides. In the following examples the velocity v_z is not taken into account.

The flow front propagation, for an isothermal Newtonian flow in a complex flat geometry

An experimental simulation with a model fluid was carried out. Basically the experimental set-up consists of two horizontal, parallel transparant plates, between which a Newtonian fluid (η = 1.13 Pas) can be injected. The fluid is injected with a constant flux (10^{-7} m^3/s) into the cavity through two holes in one of the plates. The used cavity (100x100x1.5 mm) has a circular insert. Fig. 6 shows the finite element mesh and the numerical and experimental results, indicated by solid and heavy solid lines, respectively.
The flow fronts are drawn after each time increment. The numerically obtained flow fronts, which correspond to the experimentally determined ones, are indicated by dots. The dashed

curves represent the weld lines.

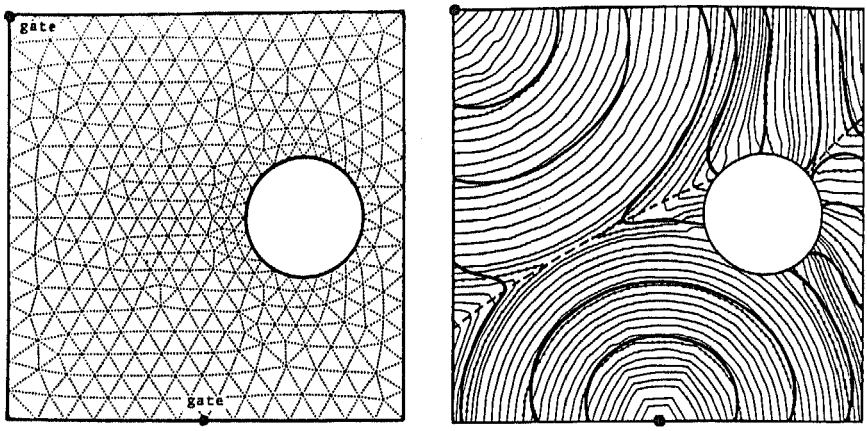

Fig. 6 Mesh, flow fronts and weld lines for two injection points

The non-isothermal filling of a complex mould with a non-Newtonian fluid

A comparison will be made between the experimental flow pattern in a mould, obtained by short shots, and the numerical simulation. In the mould a rectangular box is produced with a varying wall thickness. The experiments were carried out by DSM (Kersemakers, 1987).
Fig. 7 shows a quarter of the box. The geometry is divided into 4 sub-areas (A-D). Sub-area A has a constant wall thickness, but the other sub-areas have a linearly varying wall thickness. For adjacent sub-areas the thickness shows a discontinuity.

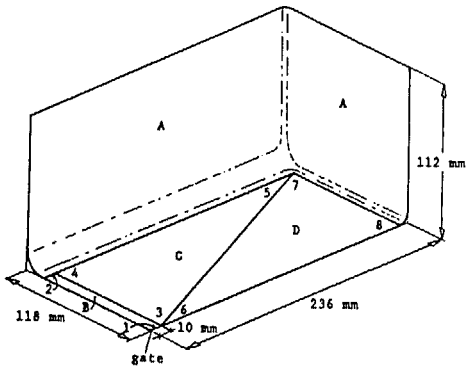

Sub-area	point/side	wall thickness (mm)
A	-	3.50
B	1	2.75
	2	3.05
C	3	2.90
	4	3.00
	5	4.20
D	6	3.80
	7	4.20
	8	4.00

Fig. 7 Quarter of the experimental mould

The mould is injected with ABS (Ronfalin FF50). The viscosity curve is fitted with the following power law model:

$$\eta = B \exp\left(\frac{A}{T}\right) \dot{\gamma}^{n-1} \qquad (17)$$

For the specific volume $\nu = 1/\rho$ the following relation is derived from the p-ν-T diagram:

$$\nu = a \exp(b(p - p_0)) + c(T - T_0) \exp(d(p - p_0)) \tag{18}$$

with separate adjustment of the parameters a, b, c and d in the solid and fluid phases. The solidification temperature T_s as a function of the pressure can be approximated quite well by a linear relationship:

$$T_s = T_0 + \alpha(p - p_0) \tag{19}$$

In the solid and the fluid regions the c_p curve is straight but has a different slope. The small peak in the transition area of the curve is taken into account by a small amount of fusion heat Γ, which is released at T_s. With a shift of T_s as a function of p it can be derived that:

$$c_p = g + h(T - T_0 - \alpha(p - p_0)) \tag{20}$$

The parameters g and h are different for the solid and the fluid phases. The heat conduction coefficient is approximated according:

$$\lambda = r + s(T - T_0 - \alpha(p - p_0)) \tag{21}$$

The material parameters are listed in Table 1.

A = 4050	K	$P_0 = 10^5$		Pa
B = 4	Pas	Γ = 2000		J/kg
n = 0.375		$\alpha = 5.4244*10^{-7}$		K/Pa
T_0 = 373	K			
	fluid phase	solid phase		
a =	$9.78*10^{-4}$	$9.78*10^{-4}$		m^3/kg
b =	$-3.86*10^{-10}$	$-2.78*10^{-10}$		1/Pa
c =	$5.53*10^{-7}$	$2.50*10^{-7}$		$m^3/(kgK)$
d =	$-4.30*10^{-9}$	$-3.74*10^{-9}$		1/Pa
g =	$1.865*10^3$	$1.555*10^3$		J/(kgK)
h =	3.44	4.47		$J/(kgK^2)$
r =	$1.75*10^{-1}$	$1.75*10^{-1}$		J/(smK)
s =	$-1.20*10^{-4}$	$-1.20*10^{-4}$		$J/(smK^2)$

Table 1 Parameters of the curve fits of ABS

The polymer is injected at a temperature of 503 K. The walls of the mould are kept at a temperature of 323 K. The total injection time equals 2.8 s. The calculated injection pressure is equal to 49.5 MPa. Fig. 8 shows the finite element mesh, the numerical and experimental results. The flow fronts are drawn after each time increment.

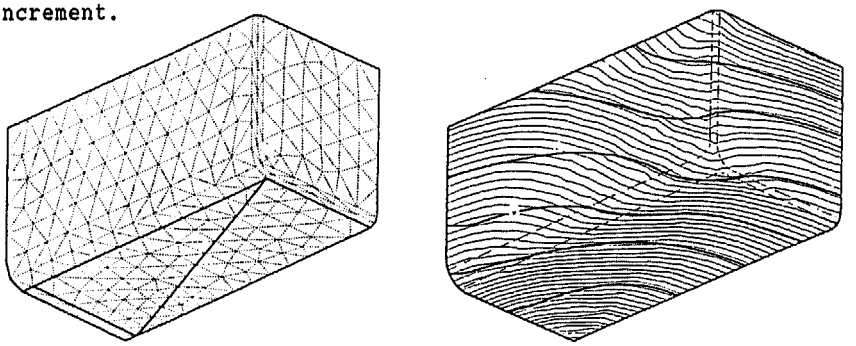

Fig. 8 Finite element mesh, numerical and experimental (heavy solid lines) flow fronts for the non-isothermal non-Newtonian case

This work is confined to viscous flow, in spite of the substantial viscoelastic effects that occur in polymer melts. Therefore, additional work with respect to these effects is desirable. A first step will be the computation of elastic stresses assuming that flow in the cavity can be determined completely from the viscous forces only. The elasticity is added afterwards, by using the calculated viscous deformation in a viscoelastic model. This approximation has to be checked by (numerical) experiments. Finally, the full set of equations that governs viscoelastic flow has to be solved. However for the time being, this goal is unattainable, because of the extensive computational effort and the number of difficulties still to be overcome in this field.

References

- Becker, E., Bürger, W.: "Kontinuumsmechanik", Teubner, Stuttgart, (1975).
- Hieber, C.A., Shen, S.F.: "A Finite-Element/Finite Difference Simulation of the Injection-Molding Filling Process", J. of Non-Newt. Fluid Mech., 7 (1980) 1-32.
- Müller, I.: "Thermodynamics", Mid-County Press, London, (1985).
- Richardson, S.: "Hele Shaw flows with a free boundary produced by the injection of fluid into a narrow channel", J. Fluid Mech., 56 (1972) 609-618.
- Schlichting, H.: "Grenzschicht-Theorie", Braun, Karlsruhe, (1982).
- Sitters, C.W.M.: "Numerical Simulation of Injection Moulding", Thesis, Eindhoven University of Technology (1988).